Resolution considerations in electro-optic, single interface deflectors

Stephen J. Barrington, Alex J. Boyland and Robert W. Eason

Optoelectronics Research Centre, University of Southampton,

Southampton SO17 1BJ, England

s.barrington@physics.org

We discuss the maximum theoretical resolution of a single interface, electro-optically controllable beam deflector in domain-engineered $LiNbO_3$ and report on experimental results for implementation of devices optimised either for maximum resolution or for maximum deflection angle. For the resolution optimised device the we observe ~50 resolvable spots for a ±1250V range, which to our knowledge is one of the highest reports of resolution/V from a solid state electro-optic beam deflector.

OCIS codes: 230.2090, 130.3120, 130.3730, 130.0130, 120.5800

1. Introduction

There is currently a tremendous interest in solid-state devices for beam scanning, deflection and switching.[1–9] Due to the demands of speed, compactness and integration, domain-engineered ferroelectrics such as $LiNbO_3$ and $LiTaO_3$ present themselves as the materials of choice. In such ferroelectrics it is possible to modify the refractive

index with an applied electric field E to achieve an induced refractive index change Δn via the electro-optic effect, as given by $|\Delta n| = \frac{1}{2}|E|r_{33}n_e^3$. The actual sign of the index change is defined by the domain orientation (direction of spontaneous polarisation) and field direction. By applying a uniform field across a domain boundary it is possible to modify the refractive index on each side of the boundary. The index difference Δn will be of equal magnitude but opposite in sign for each domain and an index contrast will occur at the domain boundary. When Snell's law is applied to this induced index boundary, deflection will occur for a beam passing through the interface region.

Since the index difference is typically small ($\sim 10^{-4}$), a common technique to increase deflection is to use multiple interfaces as shown in Fig. 1(a). Modification of this basic design[7] has been demonstrated to show significant deflection ($\sim$15°) with good beam quality. A simpler alternative has been recently demonstrated[1] and is shown in Fig .1(b). This is essentially a single interface version of the previous deflector, but increased deflection is achieved for the input beam when grazing incidence is used. By applying Snell's law (Eq. 1) it is apparent that setting θ_1 close to 90° will increase the output deflection for a given Δn.

$$\sin\theta_2 = \left(\frac{n_e + \Delta n}{n_e - \Delta n}\right)\sin\theta_1 \tag{1}$$

where θ_1 and θ_2 are as shown in Fig. 2.

The increased deflection, however, is made at the expense of increased divergence of the output beam thus reducing the resolution of the device. Overall deflection can be

a misleading quantity to determine the performance of a deflector as this could always be increased with suitable lenses. A more accurate figure of merit is the number of separate resolvable spots that can be imaged from the deflector output. This paper takes an analytical and experimental look at the achievable resolutions for a single interface deflector.

In keeping with previous work[5] we will define the resolution as:

$$N = \frac{\theta_{max}}{\theta_{div}} \tag{2}$$

where θ_{max} is total angular range of deflection and θ_{div} is the far field divergence of the beam as defined by its waist size (assuming Gaussian beam profiles). In a more general case, where the divergence may be a function of θ_1 (as is the case for a single interface close to TIR) it can be given as.

$$N = \int_0^{\theta_{max}} \frac{\mathrm{d}\theta_1}{\theta_{div}(\theta_1)} \tag{3}$$

2. The effect of the output face

It is useful at this point to establish the effect the output face has on maximum deflection and resolution. The maximum deflection angle is often given as two values: deflection achieved from the output of the device (in the far field) and deflection achieved solely by the interface or interfaces (i.e deflection achieved before the beam exits the device). The two are different since the output facet will always work to increase the achievable deflection by simple application of Snell's law. Eason *et al*[1] have angled the output facet to further increase the observed deflection from the

interface for this exact reason.

Consider a deflectable beam, as shown in Fig. 3 (deflection from $\theta_1 = 0 \rightarrow \theta_{max}$, note that in this example angles are given with respect to the interface for simplicity), in a medium of refractive index n with a fixed divergence θ_{div1}, incident upon an air interface. Before it reaches the output facet, the incident beam clearly has a resolution as described in Eq.2. After exiting the output facet, however, the beam divergence θ_{div2} is now a function of θ_1. By applying Snell's law at this point we can obtain:

$$\frac{\mathrm{d}\theta_2}{\mathrm{d}\theta_1} = n_e \frac{\cos\theta_1}{\cos\theta_2} \tag{4}$$

i.e. the angular deflection of the output beam is amplified by a factor $n_e \frac{\cos\theta_1}{\cos\theta_2}$ which becomes quite significant as the incident beam approaches the critical angle. Likewise, we can show that the divergence of the output beam is also going to similarly increase. It can be seen that the relationship between the spot sizes on either side of the interface is given by:

$$\frac{w_1}{\cos\theta_1} = \frac{w_2}{\cos\theta_2} \tag{5}$$

i.e. the waist is reduced by a factor $\frac{\cos\theta_2}{\cos\theta_1}$ It therefore follows that the divergence is multiplied by the same factor (including a refractive index term to allow for the change in medium) which gives:

$$\theta_{div2} = \theta_{div1} n_e \frac{\cos\theta_1}{\cos\theta_2} \tag{6}$$

It is assumed that this is the case regardless of whether the waist is at the interface

or not.

For this particular set-up the output resolution will be given by:

$$N = \int_0^{\theta_{max}} \frac{\mathrm{d}\theta_2}{\theta_{div2}(\theta_1)} \tag{7}$$

Substituting Eq.6 and Eq.4 into this equation now yields the same result as equation 2. This shows that the presence of the output face does not increase the number of resolvable spots. Setting the output face at an angle will also not affect the resolution. This is equivalent to starting the lower limit of the integral at a number higher than zero. The optimum angle for the output facet is at right angles to the interface as this will reduce the overall divergence of the output beam. We can now consider the resolution of the device by only looking at the deflection at the poled interface and can neglect the effect of the output facet.

3. Resolvable spots after interface

Referring to Fig. 2, if we consider the beam waist sizes at the interface: (similar to Eq. 5) and write w_2 in terms of its far field divergence, we can obtain:

$$\theta_{div} = \frac{\lambda \cos\theta_1}{w_1 \pi n_e \cos\theta_2} \tag{8}$$

Using a binomial approximation of Snell's law from Eq. 1, and substituting in $\Delta n = \frac{1}{2} E r_{33} n_e^3$ we get:

$$\sin\theta_2 = \left(1 + E r_{33} n_e^2\right) \sin\theta_1 \tag{9}$$

although here the sign change is somewhat arbitrary depending on the direction of

the z-axis of the crystal. For simplicity it will be defined as above. i.e on the output side of the interface a negative index is induced with the application of a positive field (defined here as positive E in Eq.9), which will cause the beam to swing away from the normal.

Differentiating w.r.t. E we get:

$$\mathrm{d}\theta_2 = \frac{\sin\theta_1}{\cos\theta_2}\left(n_e^2 r_{33}\right)\mathrm{d}E \tag{10}$$

We can then write the number of resolvable spots N as:

$$N = \int_{E_{min}}^{E_{max}} \frac{\mathrm{d}\theta_2(E)}{\theta_{div}(E)} \tag{11}$$

whereupon substitution of the above equations will yield:

$$N = \frac{\tan\theta_1 n_e^3 r_{33} w_1 \pi}{\lambda} \cdot \Delta E \tag{12}$$

Where $\Delta E = E_{max} - E_{min}$.

θ cannot be set arbitrarily close to 90°, however, as it is limited by the device length L and the beam waist size w_1 at the interface, as given by:

$$\Rightarrow L = \frac{2w_1}{\cos\theta_1} \tag{13}$$

It does, however show that maximum resolution is going to be achieved when the input beam is set an an angle such that it interacts with the entire length of the device. Assuming this to be the case we can substitute Eq. 13 into 12 to obtain:

$$N = \frac{\sin\theta_1 n_e^3 r_{33} L\pi}{2\lambda} \cdot \Delta E \tag{14}$$

This equation however is not entirely correct. The implication here is that the maximum resolution would be found at $\sin\theta_1 = 90°$. This obviously is not the case as at 90° the angular range of deflection before TIR is 0°. What this equation does not consider is that beyond a certain range, E_{max} (the maximum positive field strength available) is a function of θ_1.

For now we just consider the resolution available from a positive applied field. E_{max} is a constant (typically limited by either the available voltage driver or breakdown voltages of the medium) up until the point at which application of the maximum field strength just causes the beam to TIR at the interface (for clarity we will refer to this input angle as the *critical input angle*). From Snell's law, at the critical input angle (set $\sin\theta_2 = 1$ in Eq.9) we have:

$$\sin\theta_1 = \frac{1}{1 + E r_{33} n_e^2} \tag{15}$$

and substituting in 14 we get:

$$N = \frac{n_e L\pi}{\lambda} \cdot (1 - \sin\theta_1) \tag{16}$$

this gives us an equation for resolution valid for input angles θ_1 larger than the critical input angle. As expected N $\rightarrow$ 0 as $\theta_1 \rightarrow 90°$

We can now plot the number of resolvable points over a complete range of input angles to establish the optimum input angle (as shown in Fig. 4). As might be expected,

the maximum resolution is achieved at the critical input angle. It is now possible to completely define the optimum set-up in terms of more usable parameters.

The maximum resolution of any single interface deflector is given by:

$$N = \frac{n_e L\pi}{\lambda} \cdot \left[1 - \frac{1}{1 + E_{max} n_e^2 r_{33}}\right] \tag{17}$$

which for small $E_{max} n_e^2 r_{33}$, approximates to :

$$N \approx \frac{n_e^3 L\pi}{\lambda} \cdot E_{max} r_{33} \tag{18}$$

where the input angle is given by Eq.15 and from which the optimum beamsize can be deduced from the device length as given by Eq.13

If we consider applying a field in the opposite direction (i.e. causing the beam to deflect towards the normal), the same considerations do not apply as there is no critical input angle in this case. Obviously the highest resolution is going to be achieved as the beam swings across the same range of angles as in the above case. (i.e. from $\theta_1 = 90°$ to the angle set by Eq.15). It is however impossible to have $\theta_1 = 90°$ as the minimum input angle is restricted by the length of the device and the beam waist. It follows, therefore, that higher resolutions are possible by deflecting the beam away from the normal. This is only the case if the input beam is at the angle set by Eq.15 (or higher). If θ_1 is any lower then equal resolutions are achievable in either direction.

4. Experimental results

Based on this information we have set up two single interface deflectors. One is optimised for maximum beam deflection, while the other is optimised for maximum

resolution.

In the first experiment the input facet was normal to the interface direction but the output facet was at an angle of 63° to the interface normal. The device thickness was 300μm and length was 13mm. The input beam was focussed by an f = 150mm spherical lens positioned at a distance of one focal length from the centre of the crystal. The beam was s-polarised to access the higher electro-optic co-efficient. A beam profiler was used to observe the beam size and quality in the far field (475mm from the crystal output face) and ascertain the approximate resolution of the device. The laser wavelength λ was 633nm and the crystal was at room temperature. Measurements were taken every 100 volts, this being the approximate voltage required to move the beam to a separately resolvable spot. The results are shown in Fig. 5. Although in this instance the angular deflection is very large (~18° across the full range of applied fields) it is obvious that the beam is highly elliptical and thus the resolution is much less than optimum for a device of this length. Both the interface and the angled output facet act to increase the beam divergence in the deflected plane. Also visible in Fig. 5 is the large decrease in transmitted intensity as the beam is deflected towards TIR, either side of the undeflected beam (i.e TIR at the interface as the beam swings away from the normal and TIR at the output facet as it swings towards the normal). This is shown more clearly in Fig. 6.

For the second experiment the input and output facet were both normal to the interface direction. The device thickness was 300μm and its length was 10mm. The input beam was focussed by an f =300mm cylindrical lens in the horizontal plane (to utilise the full length of the interface) and an f =150mm cylindrical lens in the verti-

cal plane (to prevent unwanted diffraction effects at the crystal aperture). The lenses were placed such that the crystal was at the beam waist in both planes. Again the beam was s-polarised, the laser wavelength λ was 633nm and the crystal was at room temperature. Measurements were taken every fifty volts, this being the approximate voltage required to move the beam to a separately resolvable spot.

The results in Fig. 7 show the beam profile as the beam is shifted away from the interface normal (i.e towards TIR), while the results in Fig. 8 show the beam profile as the beam is shifted towards the interface normal. The angular divergence of the beam is as indicated in the x-axis so this is a true representation of the deflector resolution. It can be seen that there are 25 separate images in each figure, giving an approximate number of 50 resolvable spots across the 2.5kV range used. We believe this is one of the highest reports of resolution/V from a solid state electro-optic beam deflector .In Fig. 7 the images are well separated further than their resolvable distance, however the power decrease is clearly visible in the output beam and significant divergence occurs towards 1kV. In Fig. 8 the images are only just resolvable, but the output beam maintains constant divergence and power across the whole range. In both cases the resolution is almost double that of the unoptimised case. It should also be noted that the calculated maximum resolution of this device is shown in Fig. 4 and this number agrees well with that observed experimentally. This shows that there is very little beam distortion present in the output beam as this would reduce observed resolution . Since the results are not taken at exactly one resolvable spot apart (merely at a convenient voltage difference that corresponds to, on average, one separation distance) they cannot be compared exactly.

5. Increasing resolution

Analytical evaluation of the maximum resolution of the single interface deflector shows us the obvious and less obvious methods of increasing the output resolution. Using a material with a higher r_{33} electro-optic co-efficient is the most obvious, but it will be a considerable while before the material would be as inexpensive, and of consistently high quality as $LiNbO_3$ is today. Reducing the device thickness is another method (thus accessing higher field strengths by reducing the electrode distance) and we are currently investigating waveguide geometries for the deflector. Whilst it is possible to use higher voltages, this will always be limited to values below the coercive field strength of the material ($\sim$22kV/mm). Higher voltages would also limit the speed the device could operate at. One obvious improvement that can be seen from Eq.18 is to increase the device length L. Not only would this linearly increase the resolution but it would also increase output beam quality. The ray paths of a tightly focussed beam are not all incident on the device interface at the same angle thus leading to beam distortion during deflection. Since a longer device requires a much less tightly focussed beam, less distortion will occur, which will further improve resolution. Also observed in equation 18 is the cubic relation of resolution with n^3. We can simultaneously increase both the refractive index and r_{33} of $LiNbO_3$ by heating the material.[10,11] This is rather fortunate due to the existing requirement to heat a $LiNbO_3$ device operating at visible wavelengths to avoid photorefractive effects. Fig. 9 shows the maximum calculated resolution that would be expected from a device 50mm long (considered a reasonable and practical length) at three different wavelengths over a

range of temperatures. It can be seen that with suitable engineering a high resolution deflector could indeed be realised.

6. Summary

We have shown how it is possible to calculate the maximum theoretical resolution for any single interface EO deflector and shown experimental results in good agreement with the theory. The results presented here are rather similar to those seen in literature for the 'prism-type' deflector. We believe, however, that due to the simplicity of construction of the single interface device it possesses a number of advantages:

1 Poling can occur solely along the crystallographic planes giving a high quality or 'sharpness' to the interface.

2 The process is fast and inexpensive, requiring no complex lithographic masks.

3 Electrodes sizes can be far smaller than in the prism type deflector, allowing for faster switching speeds.

4 Its simplicity of design can allow for 2D beam scanning. (and we have recently submitted our results for publication[12])

Acknowledgements

The authors are grateful to the Engineering and Physical Sciences Research Council (EPSRC) for funding for AJB and grant no. GR/N00302.

References

1. R. W. Eason, A. J. Boyland, S. Mailis, and P. G. R. Smith. Electro-optically controlled beam deflection for grazing incidence geometry on a domain-engineered interface in $LiNbO_3$. *Optics Communications*, 197(1-3):201–207, 2001.

2. A. J. Boyland, S. Mailis, J. M. Hendricks, P. G. R. Smith, and R. W. Eason. Electro-optically controlled beam switching via total internal reflection at a domain-engineered interface in $LiNbO_3$. *Optics Communications*, 197(1-3):193–200, 2001.

3. A. J. Boyland, G. W. Ross, S. Mailis, P. G. R. Smith, and R. W. Eason. Total internal reflection switching in electro-optically addressable domain-engineered $LiNbO_3$. *Electronics Letters*, 37(9):585–587, 2001.

4. Y. Chiu, R. S. Burton, D. D. Stancil, and T. E. Schlesinger. Design and simulation of wave-guide electrooptic beam deflectors. *Journal of Lightwave Technology*, 13(10):2049–2052, 1995.

5. Y. Chiu, V. Gopalan, M. J. Kawas, T. E. Schlesinger, and D. D. Stancil. Integrated optical device with second-harmonic generator, electrooptic lens, and electrooptic scanner in $LiTaO_3$. *Journal of Lightwave Technology*, 17(3):462–465, 1999.

6. K. T. Gahagan, D. A. Scrymgeour, J. L. Casson, V. Gopalan, and J. M. Robinson. Integrated high-power electro-optic lens and large-angle deflector. *Applied Optics*, 40(31):5638–5642, 2001.

7. D. A. Scrymgeour, Y. Barad, V. Gopalan, K. T. Gahagan, Q. X. Jia, T. E. Mitchell, and J. M. Robinson. Large-angle electro-optic laser scanner on $LiTaO_3$

fabricated by in situ monitoring of ferroelectric-domain micropatterning. *Applied Optics*, 40(34):6236–6241, 2001.

8. D. A. Scrymgeour, A. Sharan, V. Gopalan, K. T. Gahagan, J. L. Casson, R. Sander, J. M. Robinson, F. Muhammad, P. Chandramani, and F. Kiamilev. Cascaded electro-optic scanning of laser light over large angles using domain microengineered ferroelectrics. *Applied Physics Letters*, 81(17):3140–3142, 2002.
9. J. A. Abernethy, C. B. E. Gawith, R. W. Eason, and P. G. R. Smith. Demonstration and optical characteristics of electro-optic bragg modulators in periodically poled lithium niobate in the near-infrared. *Applied Physics Letters*, 81(14):2514–2516, 2002.
10. C.J.G. Kirkby and C. Florea. Electro-optic coefficients of $LiNbO_3$. In K.K. Wong, editor, *Properties of Lithium Niobate*, volume 28 of *EMIS datareviews*, pages 136–137. IEE publishing, 2002.
11. C.J.G. Kirkby and C. Florea. Dispersion properties of $LiNbO_3$ and tables. In K.K. Wong, editor, *Properties of Lithium Niobate*, volume 28 of *EMIS datareviews*, pages 122–123. IEE publishing, 2002.
12. S. J. Barrington, A. J. Boyland and R. W. Eason. Domain engineered lithium niobate as a medium for an integrated solid-state 2D color laser scanning system. *Submitted to applied optics.*

List of Figure Captions

Fig. 1. Schematics of 2 methods of enhancing the angular deflection of EO solid state deflectors. Shaded areas indicated a domain reversed region opposite to the unshaded areas.

Fig. 2. Beam deflection from a single interface.

Fig. 3. Deflectable beam incident on an air interface.

Fig 4. Calculated maximum resolution of deflector (The dimensions and values used are coincident with those used in experimental results described later).

Fig. 5. Image showing beam profile with deflection away from interface normal. Results here are optimised for deflection, not resolution. Beam profile images are scaled with the x axis.

Fig. 6. Transmitted intensity as a function of applied voltage for the faceted deflector.

Fig. 7. Image showing beam profile with deflection away from interface normal. Beam profile images are scaled with the x axis.

Fig. 8. Image showing beam profile with deflection towards interface normal. Beam profile images are scaled with the x axis.

Fig. 9. Temperature dependence of resolution at three wavelengths roughly corresponding to Red, Green and Blue light.

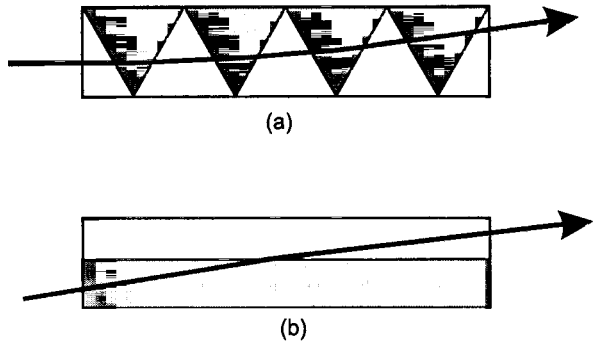

Fig. 1. Schematics of 2 methods of enhancing the angular deflection of EO solid state deflectors. Shaded areas indicated a domain reversed region opposite to the unshaded areas. barrington01.eps

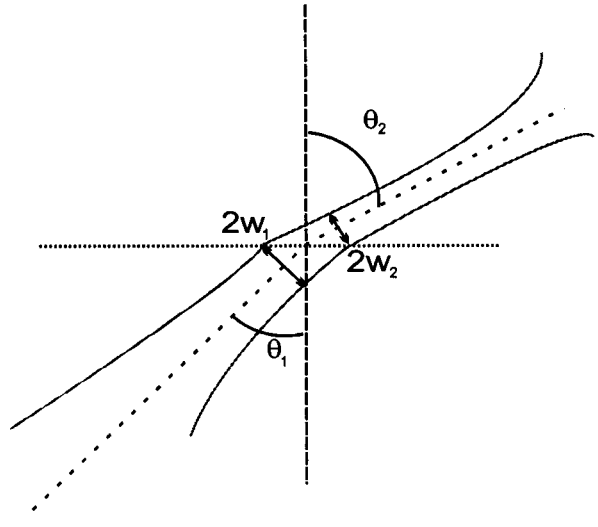

Fig. 2. Beam deflection from a single interface. barrington02.eps

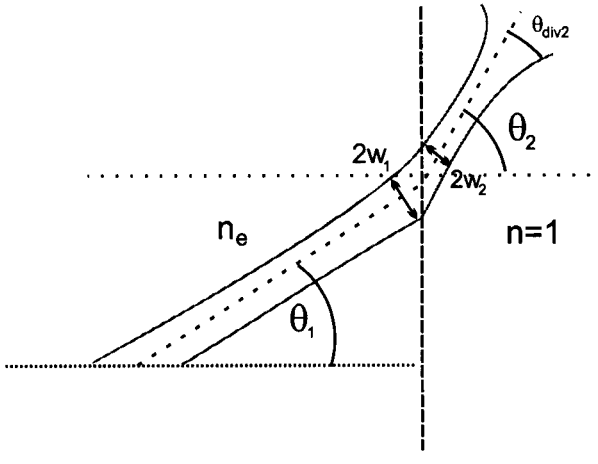

Fig. 3. Deflectable beam incident on an air interface. barrington03.eps

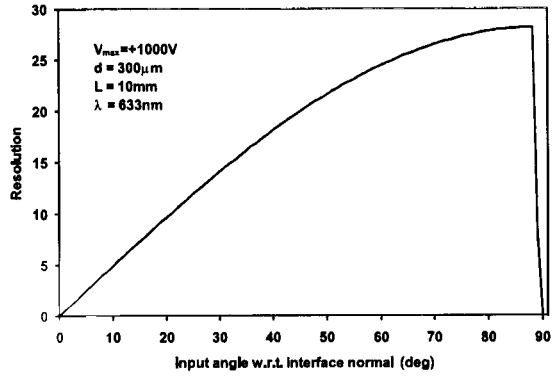

Fig. 4. Calculated maximum resolution of deflector (The dimensions and values used are coincident with those used in experimental results described later). barrington04.eps

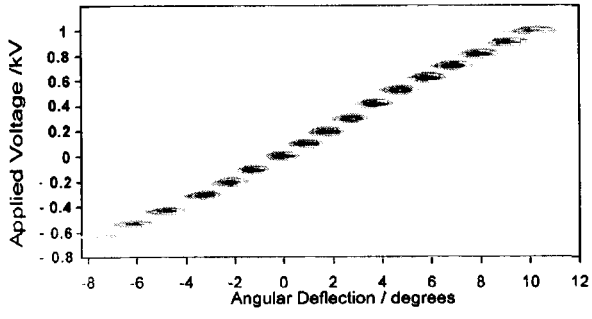

Fig. 5. Image showing beam profile with deflection away from interface normal. Results here are optimised for deflection, not resolution. Beam profile images are scaled with the x axis. barrington05.eps

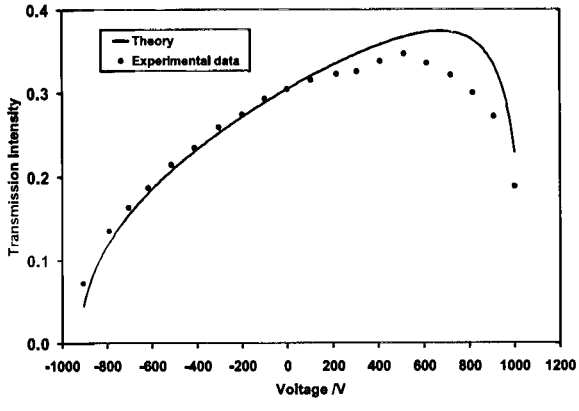

Fig. 6. Transmitted intensity as a function of applied voltage for the faceted deflector. barrington06.eps

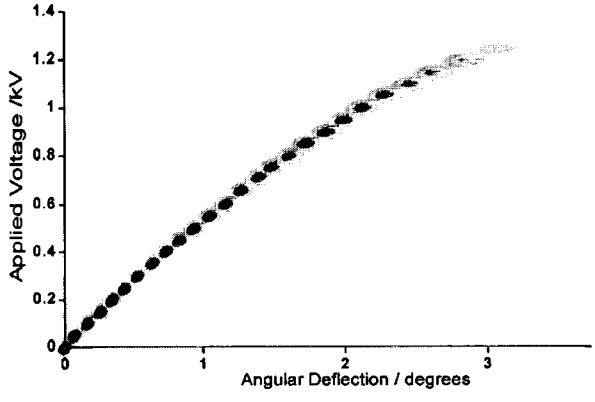

Fig. 7. Image showing beam profile with deflection away from interface normal.

Beam profile images are scaled with the x axis.barrington07.eps

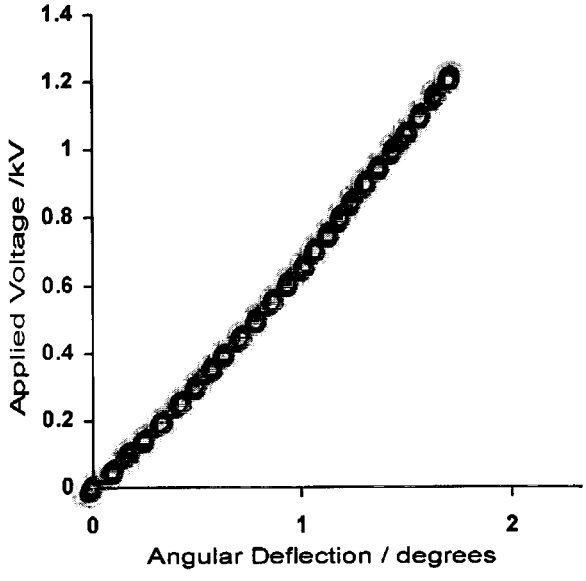

Fig. 8. Image showing beam profile with deflection towards interface normal. Beam profile images are scaled with the x axis. barrington08.eps

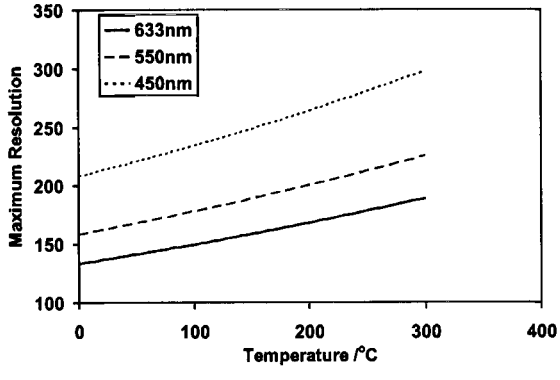

Fig. 9. Temperature dependence of resolution at three wavelengths roughly corresponding to Red, Green and Blue light. barrington09.eps